A Finite Differences-Based Metric for Magnetic Resonance Image Inpainting

Marco Seracini[1(✉)], Claudia Testa[2,3], and Stephen R. Brown[4,5]

[1] Department of Biomedical and Neruomotorial Sciences, University of Bologna, via Massarenti 9, 40138 Bologna, Italy
marco.seracini2@unibo.it
[2] IRCCS, Istituto delle Scienze Neurologiche di Bologna, via Altura 3, 40139 Bologna, Italy
claudia.testa@unibo.it
[3] Department of Physics and Astronomy "Augusto Righi", University of Bologna, viale Berti Pichat 6/2, 40127 Bologna, Italy
[4] Massachusetts Institute of Technology, 77 Massachusetts Ave, Cambridge, MA 02139, USA
srbrown@mit.edu
[5] Aprovechar Lab L3C, Montpelier, VT, USA
srbrown@aprovechar.org

Abstract. In this article, using a patch-based approach, we inpaint two different T_1 and T_2 sets of Magnetic Resonance images of phantoms by the application of a new metric formulated with the introduction of finite differences. We show that the new approach allows us to exactly reconstruct the missing part of the image, when the unknown patch is present in the search domain. Moreover, we show that higher finite difference order terms are needed when the contrast of the area to inpaint is reduced.

Keywords: Texture Synthesis · Inpainting by Patch · Image Processing

1 Introduction

In the literature, the so called *inpainting problem* consists in filling zones of missing information in an image, digitally represented by a two-dimensional discrete set [18].

To fill those areas of missing information, different approaches and solutions have been proposed and described in the literature ([2,7–9,11,14,22,26,29]). Among those, an interesting promising one was introduced by [8,29]: for each missing point in the to-be-inpainted area a suitable neighborhood of the point is scrolled all over the known image data (in what follows also referred to as search domain) and the correct value is chosen maximizing a similarity measure between the neighborhood and the given signal. The described method, despite its conceptual simplicity, provides very good results in a relatively affordable execution time [13,20,28].

Subsequently, in [7], a mathematical formalization of the algorithm has been provided through a functional, named *Inpainting Energy* (E_I). E_I quantifies the difference between a neighborhood of the missing points and the known part of the signal itself.

© The Author(s), under exclusive license to Springer Nature Switzerland AG 2023
O. Gervasi et al. (Eds.): ICCSA 2023 Workshops, LNCS 14108, pp. 608–622, 2023.
https://doi.org/10.1007/978-3-031-37117-2_41

Despite the goodness of the achieved results, these methods mask a conceptual weakness because they neglect the *under-the-surface* structural information hidden in the known part of the signal, i.e., in the structure of the surface of the image function (see Fig. 1). In fact, to evaluate the similarity between two functions (or signals) it is possible to take into account, together with their pointwise difference, also the similarity between their derivatives (or their finite differences). This structural information is therefore connected with the concept of the derivatives or, in this specific discrete case, of the finite differences [17,19,23].

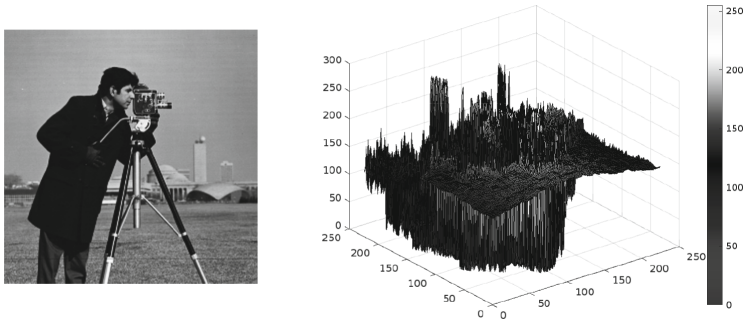

Fig. 1. Cameraman picture (on the left) and its three-dimensional representation as a surface with a two dimensional support (on the right).

For this reason, introducing a methodology that cares about these structural aspects gives support to:

- a better understanding of the logic behind the inpainting process;
- a faster convergence to a stable solution;
- better results.

Finite differences have been used in image and signal reconstruction mainly with regularization purposes [3,25,31]: this approach is based on the assumptions, sometimes arbitrary, about certain regularity properties of the signal to reconstruct. Differently, with our method we stay true to the inpainting-by-patch logic.

Moreover, the inclusion of the finite differences assures a faster convergence to the solution, supported by the evolution of the inpainting error at each iteration.

Finally, the quality of the results is improved. On one hand, in case of aesthetic needs (computer graphics, arts or photography, only to name some) to consider satisfactory the achieved results, the inpainted area has to be not *eye-distinguishable*, by a human observer, from the known part of it. This way to evaluate the quality of the reconstruction is user-dependant and completely detached from the ground truth. This approach is evidently not suitable in case of medical images that are going to be used for diagnostic purposes.

In medical cases, we require the achieved reconstructions to be representative of the effective nature of the investigated biological tissue (i.e., healthy or not). The missing of

a reference in the most of the real medical investigations, e.g., because it is not possible to perform the extraction of the suspicious tissue from the patient body, allows to test the procedure only on *ad hoc* built objects, referred to as phantoms. In particular, we:

- take the images of a set of phantoms;
- delete some zones from them;
- perform the search of the missing parts in the pristine images, such that we expect the reconstruction to be without errors of any kind;
- check the similarity between the achieved reconstructions and the pristine images.

A meaningful example of medical images is represented by the ones coming from Magnetic Resonance (MR) Imaging systems, which are widely used, e.g., for structural and functional brain investigations [12,24].

The reasons for the partial loss and degradation of the signal in MR images are artifacts due to local magnetic field inhomogeneities, due to motion, to eddy currents, to low signal to noise ratio. In particular susceptibilities variations and eddy currents can produce loss of signal in regions of the image.

To face these problems in the post processing stage, given the practical difficulties and the economic expense to repeat the MR exams on individuals, the attempts to reconstruct the missing areas have widely employed, in the recent years, various structures of Neural Networks (NN) and Deep Learning (DL) techniques [1,16,21]. The main drawback of NN-based approaches is that a complete mathematical model is missing, such that their results can not be stated to be a priori valid in general, even if they are usually visually impressive.

The goal of our work is to study how the introduction of a finite differences term in the formulation of E_I improves the quality and reliability of the reconstructions, as with general images, and in the specific MRI case.

In particular, we want to prove that the minimization of the inpainting energy, as defined in [7], is not enough to achieve back the pristine images, even if the missing parts are effectively present in the search domain. Moreover, due to the limited available number of images, our analysis is focused on *deterministic* methods only, given the impossibility to adequately train NN and DL.

The main novelties introduced in this work concern the use of the finite differences of any order (also higher than one) for the inpainting process and the experimental test of this procedure on real medical Magnetic Resonance images.

The article is structured as follows: in Sect. 2 the formalization of the algorithm is provided. The more applied part of the work is exposed in Sect. 3, and Sect. 4 where the MR dataset, the numerical implementation and the numerical results are respectively described. A final paragraph in Sect. 5 summarizes the achieved results.

2 Algorithm Formalization

Working with an n-bits coded image function I, of size $M \times N$, containing the area Ω to be inpainted (see Fig. 2), we consider a function χ of the point to inpaint. In [28,29] the mean square error (MSE) is calculated between χ and whatever plausible patch in the given image. We denote it by MSE_χ.

From the minimization of MSE_χ the value of each missing point comes (e.g., [7]). In Fig. 2 a graphical example of this procedure is provided. Anyway, this process can bring to multiple different values, such that an unique solution can not always exist. We can group these equivalent values as belonging to the same class of equivalence. To reduce the number of the values belonging to the same class, we introduce, in the computation of the value for the inpainting, a new term, taking into account of the finite differences of any order.

Then the inpainting-by-patch task can be conceptually outlined in two main sub-problems:

1. individuate the *content-driven* solutions depending on E_{C_T};
2. individuate the *structure-driven* solutions depending on E_{S_T}.

E_{C_T} is the mean square error of the signal respect with a given patch of support χ in the image; E_{S_T} is the mean square error of the signal finite differences respect with a given patch of support χ. The *content-driven* solutions are those values that minimize the MSE_χ while the *structure-driven* solutions are those ones that minimize the mean square error calculated on the finite differences. The final inpainted results come from the best possible match of both of these conditions, opportunely combined together. We denote this combination with E_T.

Moreover, to make the contribution of E_{C_T} and E_{S_T} comparable, also in the physical dimensionality sense, normalization coefficients $w_{S_k} = \frac{1}{2^k}$, where k is the order of the finite differences, are needed. Note that, in this case $\sum_{k=1}^{\infty} w_{S_k} = 1$, such that, to the limit, the contribution of the finite differences equals the contribution of the content term.

In Algorithm 1 we show the pseudo-code we have used for the calculation of the E_{C_T} and E_{S_T} contributions.

3 MR Dataset

MR images have been acquired by a 3T scanner (Siemens, Skyra) at the IRCCS Institute of Neurological Sciences, Bellaria Hospital (Italy), using a 64 channels head/neck

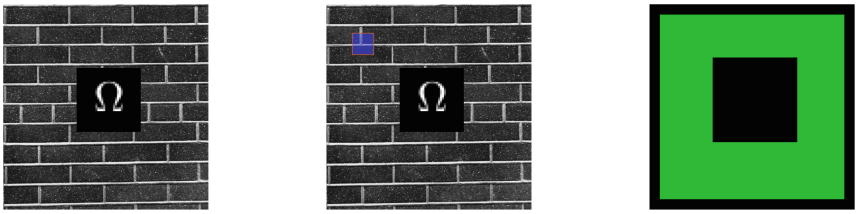

(a) I (b) I and χ (c) Valid search domain

Fig. 2. From left to right: (a) image I contianing the to-be-inpainted area Ω; (b) in blue, bordered in orange, the support of the neighborhood function χ, centered in a point of the valid search domain; (c) the green area represents the set for which the inpainting energy is well defined. The black border is half the size of χ. (Color figure online)

Algorithm 1 Pseudo-code of the algorithm used for the inpainting procedure. The value of maxint represents the maximum possible value available in the calculation system. Ts denotes the given part of the image from which the values of the missing points are deduced.

procedure INPAINT(I=Image,Ω=To-Be-Inpainted area,Ts=Training Set)

for each point of coordinates (i, j) in Ω **do**
$E_{T_{min}} = maxint$
loop :
for each point of coordinates (h, k) in Ts **do**
calculate E_{C_T}
calculate E_{S_T}
$E_T = E_{C_T} + E_{S_T}$
if $E_T < E_{T_{min}}$ **then**
$I(i, j) \leftarrow Ts(h, k)$
else
goto loop:

coil. To evaluate hardware performance and quantitative parameters (such as geometry distortion, slice thickness accuracy, intensity uniformity, ghosting artifact, and high contrast spatial resolution) of the images an ACR phantom (American College of Radiology [30]) was used. T_1 and T_2 sequences were acquired.

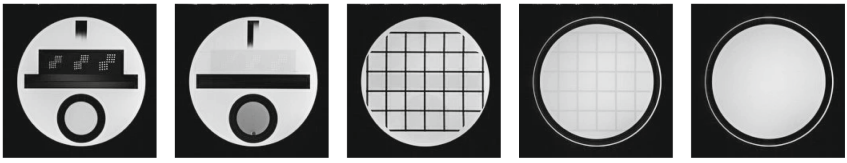

(a) T_1 n. 1; $W_C = 254$. (b) T_1 n. 2; $W_C = 254$. (c) T_1 n. 3; $W_C = 254$. (d) T_1 n. 4; $W_C = 254$.. (e) T_1 n. 5; $W_C = 254$.

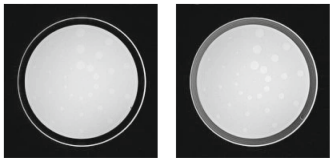

(f) T_1 n. 6; $W_C = 254$. (g) T_1 n. 7; $W_C = 254$.

Fig. 3. Set of MR acquisitions of seven different phantoms wth their W_C, T_1 sequence.

The MR T_1 sequence provides a set of better contrast images in ACR phantom, if compared with the T_2 one. For this reason, under each image in Figs. 3 and 4 we show the corresponding value of their Weber contrast, defined as follows [10]:

$$W_C := \frac{I_{max} - I_{min}}{I_{min}} .$$

Moreover, to quantify the quality of the reconstructions the Peak Signal to Noise Ratio (PSNR) has been used [27].

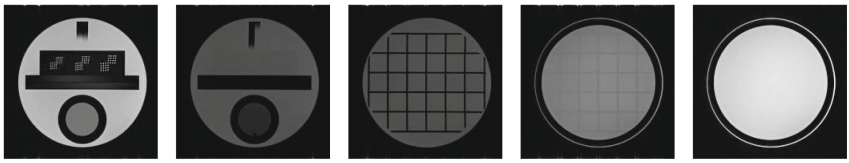

(a) T_2 n. 1; $W_C = 204$. (b) T_2 n. 2; $W_C = 79$. (c) T_2 n. 3; $W_C = 75$. (d) T_2 n. 4; $W_C = 135$. (e) T_2 n. 5; $W_C = 254$

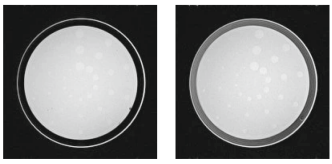

(f) T_2 n. 6; $W_C = 254$. (g) T_2 n. 7; $W_C = 254$.

Fig. 4. Set of MR acquisitions of seven different phantoms with their W_C, T_2 sequence.

Moreover, to make the contribution of E_{C_T} and E_{S_T} comparable, also in the physical dimensionality sense, we put $w_{S_k} = \frac{1}{2^k}$, that is also a theoretical set of appropriate values. Note that, in this case $\sum_{k=1}^{\infty} w_{S_k} = 1$, such that, to the limit, the contribution of the finite differences equals the contribution of the content term.

4 Numerical Results

In this section we show some meaningful numerical results achieved with and without the introduction of the finite differences. We use a square neighborhood χ of side $2L+1$.

The first example is represented by a quasi periodic texture (de Bonet's sample number 161 [6]), Ω has the size of 12×14 pixels (the black rectangle in Fig. 5).

In the same Fig. 5 the results of inpainting Ω for different values of L are shown, by only using the content-driven term (i.e., $E_T = E_{C_T}$).

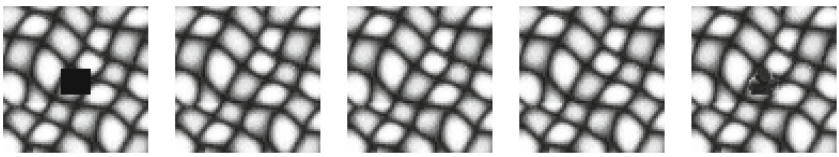

(a) Ω in black. (b) $2L + 1 = 17$ (c) $2L + 1 = 15$ (d) $2L + 1 = 13$ (e) $2L + 1 = 11$

Fig. 5. Inpainting of Ω by mean of $E_T = E_{C_T}$, for different values of $2L + 1$. In (a) the image to inpaint with Ω in black. Then, (b) to (e), the results after the inpainting with $2L+1 = 17, 15, 13, 11$ respectively. The minimum value that visually guarantees a suitable final result is $2L+1 = 13$. We stress that all the reconstructions achieved for different values of $2L+1$ are numerically different, even if to the naked eye they look visually identical.

From the same figure we can see that increasing the support of the neighborhood χ until $2L+1 = 13$, the reconstruction quality improves. On the other hand, for $2L+1 > 13$ the final images appear visually equivalent.

On the contrary, by using $E_T = E_{C_T} + E_{S_T}$, even the case $2L + 1 = 11$ results in a correct reconstruction, as shown in Fig. 6.

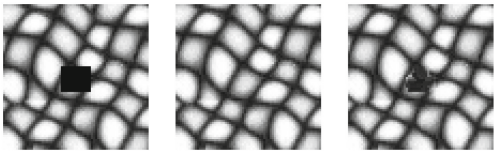

(a) Ω in black. (b) $l = 1$ (c) $l = 0$

Fig. 6. From left to right: (a) image to be inpainted with Ω of size 12×14 pixels; (b) inpainting result using $E_T = E_{C_T} + E_{S_T}(l = 1)$; (c) inpainting result using $E_T = E_{C_T}$ only. Both the reconstructions have been performed with $2L + 1 = 11$. The better performance deriving from the contribution of E_{S_T} is visually evident.

In [7] they formulated the expression of the inpainting energy and showed that it has a decreasing trend. To evaluate the behavior of the minimization of the functional when introducing the finite differences we recorded the values of $E_T = E_{C_T} + E_{S_T}$ at each iteration. Its trend is converging faster to a lower minimum than the case not using the finite differences; the trend exhibits also less oscillations and a higher rate of regularity of the convergence process (see Figs. 8 and 11).

The same tests, performed increasing the size of Ω to 41×41 pixels, result in what shown in Fig. 7. The associated energy trends are in Fig. 8.

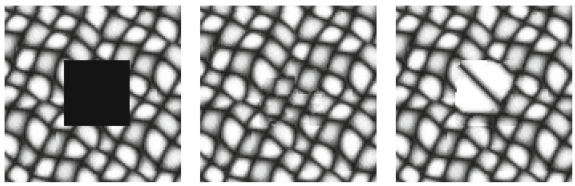

(a) Ω in black. (b) $E_T = E_{C_T} + E_{S_T}$ (c) E_{C_T}

Fig. 7. (a) Initial Ω, size 41×41 pixels; (b) inpainting result using $E_T = E_{C_T} + E_{S_T}$ (first order finite differences); (c) inpainting result using E_{C_T} only. Both the reconstructions have been performed with $2L + 1 = 11$. The better performance deriving from the introduction of E_{S_T} is, again, visually evident.

Further examples of reconstruction of images, taken from the Brodatz database [4], are available in Fig. 9 and 10, together with their energy trends (see Fig. 11 again).

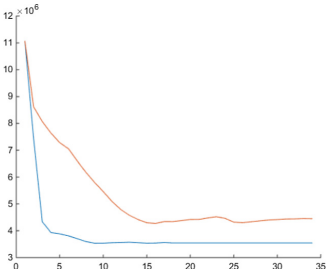

Fig. 8. The figure shows two E_T trends when varying L: in red $E_T = E_{C_T}$, in blue $E_T = E_{C_T} + E_{S_T}$. The contribution of the finite differences brings to a faster and more regular convergence to the minimum value.

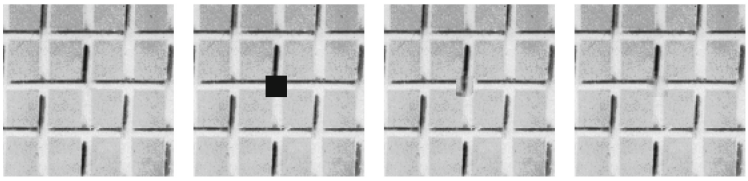

(a) Pristine I. (b) Ω in black. (c) $E_T = E_{C_T}$. (d) $E_T = E_{C_T} + E_{S_T}$.

Fig. 9. Inpainting of texture D1 taken from Brodatz database with $2L + 1 = 23$. From left to right: (a) pristine image; (b) image to be inpainted (Ω in black, size 16×16); (c) inpainting by mean of $E_T = E_{C_T}$ and (d) $E_T = E_{C_T} + E_{S_T}$. The result achieved using the first order finite difference are visually closer to the pristine image with respect to the case when the finite differences have not been used. (Color figure online)

In Fig. 9 the result achieved introducing the structural term appears free from shadowing artifacts: in this case the pristine image has not been used as search domain, such that a perfect (i.e.,with zero error) reconstruction is not generally possible.

In Fig. 10 the result achieved introducing the finite differences appears more compliant with the geometrical structure of the texture, if compared with the images obtained using content-driven only.

From the previous considerations we can infer that the introduction of E_{S_T} allows us to carry more structural information in the final reconstruction.

After these general examples we have tested the effects of introducing the finite differences in MR phantom images and we have compared the achieved results with the ones coming from the Matlab function *inpaintExamplar*, based on [5,15] and generally taken as reference in the inpainting-by-patch-approach. In the follwing examples the pristine image has been used as search domain for the determination of the best value to inpaint. Only in those cases, when the missing part in Ω is contained in the image itself (or in the used search domain), a zero-error reconstruction is possible (e.g., in a

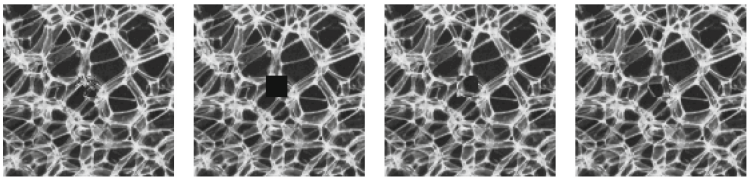

(a) Pristine I. (b) Ω in black. (c) $E_T = E_{C_T}$. (d) $E_T = E_{C_T} + E_{S_T}$.

Fig. 10. Inpainting of texture D111 taken from Brodatz database with $2L + 1 = 27$. From left to right: (a) pristine image; (b) image to be inpainted (Ω in black, size 16×16); (c) inpainting by mean of $E_T = E_{C_T}$ and (d) $E_T = E_{C_T} + E_{S_T}$. The result achieved using the first order finite difference are visually closer to the pristine image with respect to the case when the finite differences have not been used. (Color figure online)

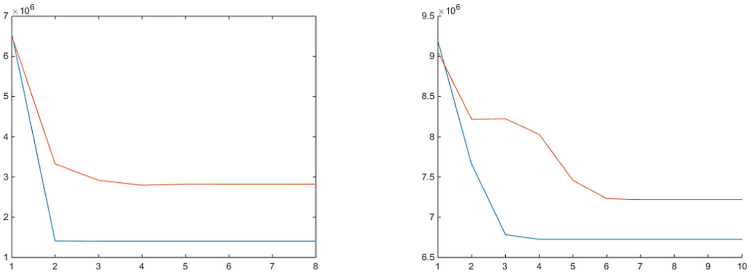

(a) D1. (b) D111.

Fig. 11. The figure shows the E_T trends: in red $E_T = E_{C_T}$, in blue $E_T = E_{C_T} + E_{S_T}$ $l = 1$. From left to right: (a) image D1 from Brodatz database; (b) image D111 from Brodatz database. Including finite differences determines a faster and more regular convergence to a lower minimum value. (Color figure online)

periodic pattern). This property is strongly auspicable because such a kind of behavior guarantees that, if the zero minimum exists for the functional, the algorithm is capable to converge to it. Viceversa, if the algorithm is not capable to reach the absolute minimum, in those case when it exists, we have, a priori, less control on the quality of the final reconstruction.

In Fig. 12 we show the reconstructions of the T_1 sequence dataset of phantoms. The inpainting performed introducing the finite differences contributions allows us to reconstruct the pristine image without errors of any kind, given a suitable order of the finite difference l. On the other hand, in the case of [5,15] the reconstructions appear sometimes to be visually not correct (see the first column M_{Dt} image), other times not identical to the pristine image. To quantify the quality of the reconstruction the values of the PSNR are shown in Table 1. For this set of images, all having the same maximum contrast $W_C = 254$, the finite differences of the first order are enough to perfectly reconstruct the original image.

Table 1. Values of the PSNR for the reconstructions of the T_1 dataset. In the T_1# columns the number of the phantom (from 1 to 7); in the Method columns the used method to inpaint, e.g., without the contribution of the finite differences [5,15] and with their contributions $E_T = E_{C_T} + E_{S_T}$; in the W_C columns the Weber contrast for the area to be inpainted, calculated in the pristine image; in the l columns the finite differences order used to inpaint; in the last columns the PSNR. In this case, where all the images have maximum contrast $W_C = 254$, $l = 1$ is enough to perfectly reconstruct the pristine image.

T_1#	Method	W_C	l	PSNR	T_1#	Method	W_C	l	PSNR
1	[5, 15]	254	0	9.286	5	[5, 15]	254	0	20.882
1	$E_T = E_{C_T} + E_{S_T}$		1	$+\infty$	5	$E_T = E_{C_T} + E_{S_T}$		1	$+\infty$
2	[5, 15]	254	0	15.943	6	[5, 15]	254	0	37.759
2	$E_T = E_{C_T} + E_{S_T}$		1	$+\infty$	6	$E_T = E_{C_T} + E_{S_T}$		1	$+\infty$
3	[5, 15]	254	0	29.932	7	[5, 15]	254	0	32.060
3	$E_T = E_{C_T} + E_{S_T}$		1	$+\infty$	7	$E_T = E_{C_T} + E_{S_T}$		1	$+\infty$
4	[5, 15]	254	0	36.752					
4	$E_T = E_{C_T} + E_{S_T}$		1	$+\infty$					

In Fig. 13 the reconstructions of the T_2 dataset of phantoms are shown. Also in this case, the inpainting performed introducing the finite differences contributions allows to reconstruct the pristine image without errors of any kind, given a suitable order of the finite difference l. Differently from the T_1 sequence, for this set of images the value of W_C is lower, according to the properties of the T_2 sequence, such that it is necessary to introduce a higher order of finite differences, to guarantee a zero error reconstruction of the pristine image.

The values of the PSNR for the achieved reconstructions are shown in Table 2. Given the lower contrast with respect to the analogous T_1 acquisitions, a higher order of finite differences l is needed to correctly reconstruct the pristine image. The most demanding case is the phantom number 3, having the lower contrast $W_C = 75$ in the whole dataset.

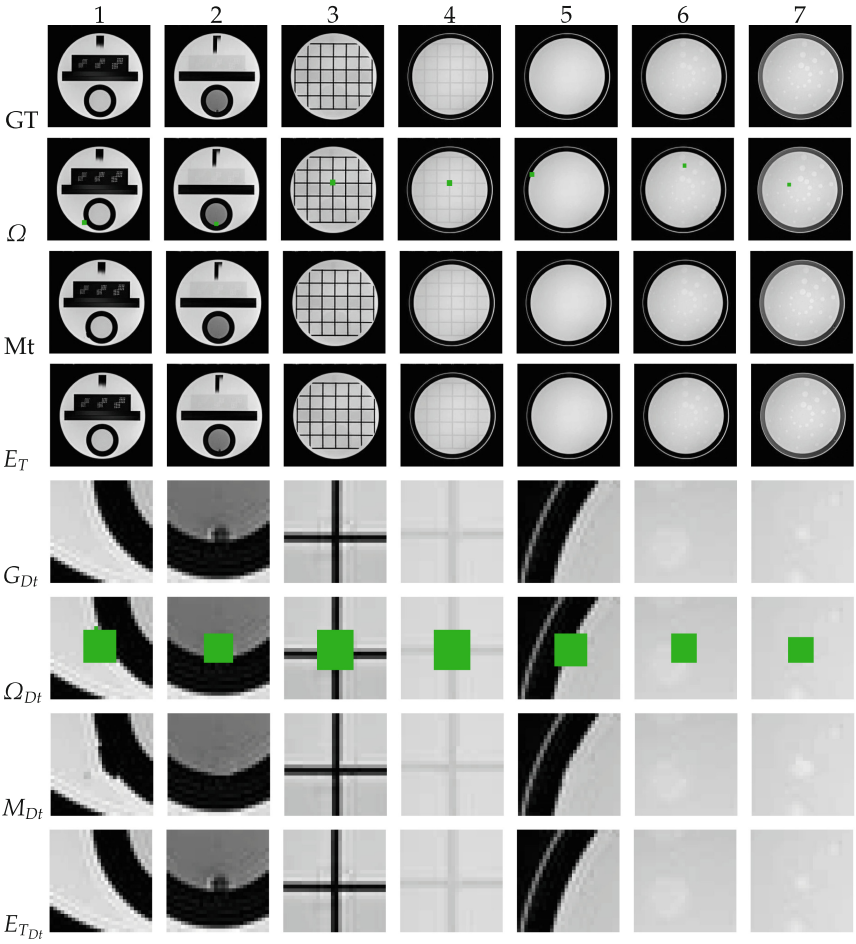

Fig. 12. Reconstructions of the set of MR acquisitions of seven different phantoms, T_1 sequence. From the first row: ground truth (GT); the area to be inpainted in green (Ω); inpainted result by [5,15] (Mt), i.e., with no contribution of the finite differences; inpainted result by the introduction of E_{S_T} in E_T (E_T); magnification of GT (G_{Dt}); magnification of Ω (Ω_{Dt}); magnification of Mt (M_{Dt}); magnification of E_T ($E_{T_{Dt}}$). For every image we used $l = 1$.

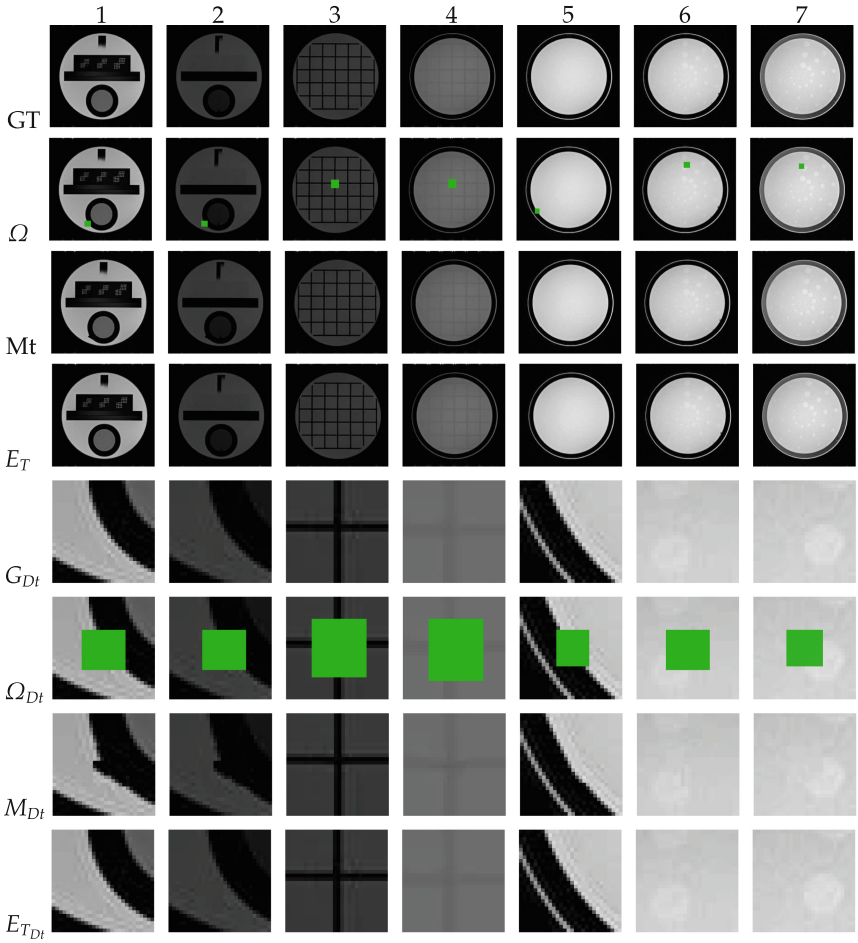

Fig. 13. Reconstructions of the set of MR acquisitions of seven different phantoms, T_2 sequence. From the first row: ground truth (GT); the area to be inpainted in green (Ω); inpainted result by [5, 15] (Mt), i.e., with no contribution of the finite differences; inpainted result by the introduction of E_{S_T} in E_T (E_T); magnification of GT (G_{Dt}); magnification of Ω (Ω_{Dt}); magnification of Mt (M_{Dt}); magnification of E_T ($E_{T_{Dt}}$). The value chosen for l varies according to W_C: lower the contrast, higher l. The values of l are available in Table 2.

Table 2. Values of the PSNR for the reconstructions of the T_2 dataset. In the T_1# columns the number of the phantom (from 1 to 7); in the Method columns the used method to inpaint, e.g., without the contribution of the finite differences [5,15] and with their contributions $E_T = E_{C_T} + E_{S_T}$; in the W_C columns the Weber contrast for the area to be inpainted, calculated in the pristine image; in the l columns the finite differences order used to inpaint; in the last columns the PSNR. In case of images with low contrast a higher order of finite differences l is needed.

T_2#	Method	W_C	l	PSNR	T_2#	Method	W_C	l	PSNR
1	[5,15]	204	0	12.009	4	[5,15]		0	45.821
1	$E_T = E_{C_T} + E_{S_T}$		1	$+\infty$	4	$E_T = E_{C_T} + E_{S_T}$	135	1	61.0568
2	[5,15]	79	0	21.229	4	$E_T = E_{C_T} + E_{S_T}$	254	2	$+\infty$
2	$E_T = E_{C_T} + E_{S_T}$		1	$+\infty$	5	[5,15]		0	18.368
3	[5,15]	75	0	38.858	5	$E_T = E_{C_T} + E_{S_T}$		1	$+\infty$
3	$E_T = E_{C_T} + E_{S_T}$		1	59.1454	6	[5,15]		0	35.364
3	$E_T = E_{C_T} + E_{S_T}$		2	59.6284	6	$E_T = E_{C_T} + E_{S_T}$	254	1	$+\infty$
3	$E_T = E_{C_T} + E_{S_T}$		3	$+\infty$	7	[5,15]		0	33.181
3	$E_T = E_{C_T} + E_{S_T}$		3	$+\infty$	7	$E_T = E_{C_T} + E_{S_T}$	254	1	$+\infty$

5 Conclusions

The achieved results show that the introduction of the finite differences terms improves the quality of reconstruction.

In particular, the new functional converges numerically faster to a lower minimum when compared with the case that does not include the finite differences. In addition, the convergence appears to be more regular and to have less oscillations.

Moreover, when the missing part of the image is available in the search domain, the finite differences term allows to achieve results without errors of any kind, i.e., identical to the pristine images. This goal can generally not be achieved using current inpainting-by-patch implementation that does not employ finite differences. This aspect is particular important to guarantee the algorithm to reach the absolute minimum, when it is available in the search domain. This importance increases considerably in case of medical diagnostic images.

In addition, our results show that lower is the contrast of the image to reconstruct, higher is the order of the finite differences needed to achieve back the pristine image. To the best of our knowledge it is the first time that finite differences are used to inpaint using an inpainting-by-patch approach. Even if in some cases the reconstruction not using the finite differences provides visually acceptable results, what achieved is not congruent with the ground truth, point that is crucial for medical images.

This behavior depends on the fact that the number of the candidate, i.e., of the metrically equivalent patches to inpaint, increase as the contrast decreases. The contribution of higher finite differences is needed to add constraints and prune the number of equivalent candidates, consequently reducing the probability to generate errors.

References

1. K. Armanious, Y. Mecky, S. Gatidis, B. Yang, Adversarial inpainting of medical image modalities, in ICASSP 2019–2019 IEEE International Conference on Acoustics, Speech and Signal Processing (ICASSP), pp. 3267–3271 (2019)
2. Ashikhmin, M.: Synthesizing natural textures. In: The proceedings of 2001 ACM Symposium on Interactive 3D Graphics, pp. 217–226 (2001)
3. Brezis, Haim: Functional Analysis, Sobolev Spaces and Partial Differential Equations. Springer, New York (2011). https://doi.org/10.1007/978-0-387-70914-7
4. Brodatz, P.: Textures: A Photographic Album for Artists and Designers. Dover, New York (1996)
5. Crimisi, A., Perez, P., Toyama, K.: Region filling and object removal by exemplar-based image inpainting. IEEE Trans. Image Process. **13**(9), 1200–1212 (2004)
6. De Bonet, J.S.: Multiresolution sampling procedure for analysis and synthesis of texture images. In: SIGGRAPH 1997 Conference Proceedings, pp, 361–368 (1997)
7. Demanet, L., Song, B., Chan, T.: Image Inpainting by Correspondence Maps: a Deterministic Approach, Applied and Computational Mathematics, 1100 (2003)
8. Efros, A., Freeman, W.T.: Image quilting for texture synthesis and transfer. In: Proceedings of SIGGRAPH 2001, pp. 341–346 (2001)
9. Efros, A.A., Leung, T.K.: Texture synthesis by non-parametric sampling. In: Proceedings of the International Conference on Computer Vision, vol. 2, pp. 1033–1038 (1999)
10. Fechner, G.T.: Elemente der Psychophysik [Elements of psychophysics], vol. 2 (1860)
11. Gatys, L., Ecker, A.S., Bethge, M.: Image texture synthesis using convolutional neural networks. In: Advances in Neural Information Processing Systems 28 NIPS 2015 (2015)
12. Evangelisti, S., et al.: Brain functional MRI responses to blue light stimulation in Leber's hereditary optic neuropathy. Biochem. Pharmacol. **191**(114488) (2021)
13. Gersho, A., Gray, R.M.: Vector Quantization and Signal Compression. Kluwer Academic Publishers (1992)
14. Hertzmann, A., Jacobs, C.E., Oliver, N., Curless, B., Salesin, D.H.: Image analogies, SIGGRAPH 2001 Proceedings of the 28th Annual Conference On Computer Graphics And Interactive Techniques, pp. 327–340 (2001)
15. Le Meur, O., Ebdelli, M., Guillemot, C.: Hierarchical super-resolution-based-inpainting. IEEE Trans. Image Process. **22**(10), 3779–3790 (2013)
16. Manjón, J.V., et al.: Blind MRI brain lesion inpainting using deep learning. In: Burgos, N., Svoboda, D., Wolterink, J.M., Zhao, C. (eds.) Simulation and Synthesis in Medical Imaging. SASHIMI 2020. LNCS. vol. 12417. Springer, Cham (2020). https://doi.org/10.1007/978-3-030-59520-3_5
17. Marr, D., Hildreth, E.: Theory of edge detection. Proc. Royal Soc. London **B-207**, 187–217 (1980)
18. Masnou, S., Morel, J.: Level lines based disocclusion. In: Proceedings 1998 International Conference on Image Processing, ICIP 1998, vol. 3, pp. 259–263 (1998)
19. Mumford, D., Shah, J.: Optimal approximations by piecewise smooth functions and associated variational problems. Comm. Pure Applied. Math. **42**, 577–685 (1989)
20. Nene, S., Nayar, S.: A simple algorithm for nearest neighbor search in high dimensions. IEEE Trans. Pattern Anal. Mach. Intell. **19**, 989–1003 (1998)
21. Nguyen, B., et al.: Unsupervised region-based Anomaly detection in brain MRI with With Adversarial Image Inpainting. In: 2021 IEEE 18th International Symposium on Biomedical Imaging (ISBI), Nice, France, pp. 1127–1131 (2021)
22. Portilla, J., Simoncelli, E.: Texture characterization via joint statistics of wavelet coefficient magnitudes. In: Fifth International Conference on Image Processing, vol. 1, pp. 62–66 (1998)

23. Rudin, L., Osher, S., Fatemi, E.: Nonlinear total variation based noise removal algorithms. Phys. D **60**, 259–268 (1992)
24. Testa, C., et al.: Stridor-related gray matter alterations in multiple system atrophy: A pilot study. Parkinsonism Relat. Disord. **62**, 226–230 (2019)
25. Tikhonov, A.N., Arsenin, V.Y.: Solutions of Ill-Posed Problems. Wiley, New York (1977)
26. Vese, L.A.: Modeling textures with total variation minimization and oscillating patterns in image processing. J. Sci. Comput. **19**(1–3), 553–572 (2003)
27. Wang, Z., Bovik, A.C.: Mean squared error: Love it or leave it? A new look at signal fidelity measures. IEEE Signal Process. Mag. **26**(1), 98–117 (2009)
28. Wei, L.: Deterministic texture analysis and synthesis using tree structure vector quantization. In: XII Brazilian Symposium on Computer Graphics and Image Processing, pp. 299–308 (1999)
29. Wei, L.Y., Levoy, M.: Fast texture synthesis using tree-structured vector quantization. In: Proceedings of SIGGRAPH 2000, pp. 479–488 (2000)
30. Weinreb, J., Wilcox, P.A., Hayden, J., Lewis, R., Froelich, J.: ACR MRI accreditation: yesterday, today, and tomorrow. J. Am. Coll. Radiol. **2**(6), 494–503 (2005)
31. Wilson, D.L., Baddeley, A.J., Owens, R.A.: A new metric for grey-scale image comparison. Int. J. Comput. Vision **24**(1), 5–17 (1997)